Pattern–Color Separable Pathways Predict Sensitivity to Simple Colored Patterns

ALLEN B. POIRSON,*† BRIAN A. WANDELL*

We have studied how contrast threshold sensitivity depends jointly on pattern and color. We measured sensitivity to colored Gabor patches from 0.5 to 8 c/deg. At each spatial frequency, we measured in many different color directions. We analyze the sensitivity measurements using a series of nested models. We conclude that a model consisting of three pattern–color separable mechanisms predicts detection performance nearly as well as fitting psychometric functions independently. We derive the pattern and color sensitivities of the separable mechanisms from the experimental data. Two derived mechanisms are spatially lowpass and spectrally color-opponent. The third mechanism is spatially bandpass and spectrally broadband.

Separability   Detection   Spatial vision   Color vision

1. INTRODUCTION

What is the relationship between the visual representation of color and other perceptual attributes? To the extent that pattern, color, time and motion are psychological representations of separate physical properties, independence of the neural representation of these physical properties is desirable. But, there is considerable evidence showing that the neural representations of these properties interact (see e.g. Wandell, 1995, Chaps 9 and 10). In an earlier paper we reported and analyzed the interactions of pattern and color using a color appearance task (Poirson & Wandell, 1993). Here, we generalize that analysis using sensitivity measurements.

Our experimental measurements and theoretical treatment are organized around the question of whether the visual mechanisms that limit contrast sensitivity are *pattern–color separable*. A mechanism is pattern–color separable when (a) its relative pattern sensitivity is invariant as we change the test stimulus' spectral composition, and (b) its relative wavelength selectivity is invariant when we change the test stimulus' spatial pattern. The absolute level of the pattern and color sensitivity can vary, but the relative pattern and color sensitivities must not. From this definition, it is evident that pattern–color separability is required before we can say that a mechanism has a unique pattern or wavelength sensitivity function. Pattern–color separability stands in contrast to a variable tuning hypothesis which states that

*Department of Psychology, Stanford University, Stanford, CA 94305, U.S.A.
†Present address: Howard Hughes Medical Institute, Center for Neural Science, New York University, 4 Washington Place, Room 809, New York, NY 10003, U.S.A.

a mechanisms's color responsivity changes with changes in stimulus parameters (Hood & Finkelstein, 1983; Finkelstein & Hood, 1984).

Separability itself is an important characteristic of a system. If it holds, then we are able to predict completely some aspect of behavioral performance or a neural mechanism with relatively few measurements. Separability is especially important if we wish to relate behavioral and physiological measurements. If we would like to compare, for example, a behavioral contrast sensitivity function with a neural contrast sensitivity function we must have some confidence that each of these contrast sensitivity functions is associated firmly with the behavior or the neural mechanism.

An important organizational principle in physiological work is the notion of functional specialization which asserts that specific regions in the brain process one aspect of the visual stimulus regardless of other visual attributes. This statement is probably not true in detail, but serves to guide experiments. We know that there are many important sites in the visual pathways where pattern and color are not represented separably. For example, the responses of primate lateral geniculate neurons are not pattern–color separable. The spatial receptive field of a red-center green-surround neuron will be very different if one measures using a long-wavelength light vs a middle-wavelength light (see Wiesel & Hubel, 1966; Gouras, 1968; Derrington, Krauskopf & Lennie, 1984). To the extent that we can explain behavioral sensitivity measurements as being mediated by separable mechanisms, then we can exclude these neural elements as being the limiting stage of contrast sensitivity.

In many behavioral studies of spatiochromatic sensitivity, pattern–color separability has been assumed

implicitly. A typical approach to measuring the spatial sensitivity of chromatic mechanisms is (a) to select the wavelength composition of a target in order to isolate the response of a putative visual mechanism, and then (b) to measure the contrast sensitivity function using this stimulus. The measured contrast sensitivity function is reported as the putative visual mechanisms' spatial sensitivity (e.g. van der Horst & Bowman, 1969; Granger & Heurtley, 1973; Mullen, 1985). This characterization is complete only if there is some reason to believe that the visual mechanism is pattern–color separable, because only in that case does a unique contrast sensitivity function exist.

In our earlier work (Poirson & Wandell, 1993; Wandell, 1995) we showed that color appearance depends on spatial pattern. Hence, taken as a whole no pattern–color separable model can predict color appearance. Even though behavior as a whole is not pattern–color separable, it is possible that the separate visual mechanisms that comprise the system are. The simplicity of the component mechanisms can be hidden if we measure after the separable pathways are combined. Again, neurons in the lateral geniculate can serve as an example. The receptive fields of these cells are conventionally modeled as the sum of a center and surround. Both the center and the surround are assumed to be pattern–color separable (Marr, 1982; Ingling & Martinez, 1985). Yet, the response of the entire cell, formed from the sum of the center and surround components, is not pattern–color separable. In the same way, the individual visual mechanisms that combine to determine the observer's representation of color and pattern may each be pattern–color separable, even though the observer's behavior is not.

Pattern–color separability is a key property because only when it holds can we be confident that the pattern and color sensitivities we measure are general descriptions of the system. Changing an unrelated stimulus parameter, such as the wavelength composition of the test light, should not produce a different contrast sensitivity function. Our approach to analyzing the representation of pattern and color is somewhat like that of Noorlander and Koenderink (1983). These authors report sensitivity measurements for stimuli at a variety of spatial and temporal frequencies, a few adaptational states, and with a variety of color directions. They considered several line-element models to predict the set of sensitivity measurements. We too measure sensitivity to a variety of colored spatial patterns. Our measurements were made on a neutral background using a slow timecourse meant to be similar to steady viewing of the stimulus. Our analysis differs from theirs in that we have focussed our measurements on determining whether performance can be explained by combining the sensitivity of a few pattern–color separable mechanisms and estimating the pattern and wavelength sensitivities of these mechanisms.

We have found that it is possible to predict accurately sensitivity to our spatiochromatic measurements using a set of three pattern–color separable visual mechanisms. The pattern and color sensitivities of the visual mechanisms that we derive from our data have an opponent-colors organization that is generally similar to the opponent-sensitivities reported in hue cancellation experiments and similar to the estimated color mechanisms derived from our color appearance studies. Consequently, we believe that our focus on the issue of separability is well-placed and that analysis of separability may prove fruitful in formulating questions about the visual representations of other perceptual variables as well.

2. METHODS

2.1. Stimuli

Space. Our spatial stimuli were vertical cosinusoids multiplied by a Gaussian window. The spatial profile of our stimuli is defined by the equation

$$S(x,y) = \exp[-(x^2 + y^2/\sigma^2{}_S)]\cos(2\pi f x). \qquad (1)$$

The parameter f defines the spatial frequency and σ_S defines the Gaussian spatial window size. We collected two complete data sets using slightly different spatial stimuli. In the *constant cycle* condition the size of the Gaussian spatial window decreased with increasing frequency so that the number of spatial cycles was constant for all test patterns. In this condition the frequencies were 0.5, 1, 2 and 4 c/deg and the width of the Gaussian window at half height subtended 7.5, 3.8, 1.9 and 0.9 degrees respectively. In the *constant size* condition we fixed the half height width of the Gaussian window to 1.5 degrees, and measured sensitivity to cosinusoids at 0.5, 1, 2, 4 and 8 c/deg.

Color. We presented our stimuli on a calibrated color monitor. We represent the test patterns in a color space defined by the Smith–Pokorny cone fundamentals (L, M, S) (Smith & Pokorny, 1975; Boynton, 1979). We use a version of the cone fundamentals in which each spectral responsivity is normalized to a peak value of 1.0. The (L, M, S) value of the uniform background in units of (microwatts/cm²-nm-sr) was $\mathbf{B} = (82.87, 65.45, 25.80)$ in the constant cycle condition and $\mathbf{B} = (7.67, 7.20, 6.31)$ in the constant size condition. These values are proportional to the quantal absorption rate of the three cone photoreceptors due to the uniform background for a standard observer. The backgrounds in both experimental conditions appeared a neutral white color. Using CIE 1931 XYZ fundamentals the background was $(xyY = 0.38, 0.39, 536.2$ c/deg m²) in the constant cycle condition and $(xyY = 0.27, 0.30, 49.8$ c/deg m²) in the constant size condition.

We represent the color coordinate of the test stimulus as a three dimensional vector, s. Each entry in the vector specifies the percent modulation of a cone type with respect to the uniform background, $\mathbf{s} = (\Delta L/L, \Delta M/M, \Delta S/S)$. This is the color representation in cone-contrast space. It is convenient to define two additional terms to represent the stimulus. First, we define the test pattern

stimulus strength to be the vector-length of the test pattern color representation in cone-contrast space

$$\|\mathbf{s}\| = [(\Delta L/L)^2 + (\Delta M/M)^2 + (\Delta S/S)^2]^{1/2}. \qquad (2)$$

Second, we define the *color direction* of a test pattern to be the corresponding unit length vector in cone-contrast space, $\bar{\mathbf{s}} = \mathbf{s}/\|\mathbf{s}\|$. Specifying the test pattern color direction and stimulus strength is equivalent to specifying the test pattern cone-contrast values.

Time. The stimulus signal was increased and decreased smoothly using a Gaussian temporal envelope

$$T(t) = \exp[-(t^2/\sigma^2_T)]. \qquad (3)$$

The width of the Gaussian at half height equaled 165 msec (duration $= \pm 2.5\sigma_T$). The complete spectral, temporal and spatial description of our stimuli is then

$$sT(t)S(x, y) + \mathbf{B}. \qquad (4)$$

One subject, HT, collected data in both the constant cycle and the constant size conditions. Our second subject, LW, participated in the constant size condition. We continuously monitored data collection and chose new color directions to reduce the uncertainty in the estimated model parameters, as described later.

2.2. Experimental apparatus

The constant cycle condition. We displayed stimuli on a Barco color monitor (model CDCT 6351) running at 87 Hz noninterlaced controlled by a Number Nine Graphics System video board (model Revolution) in an IBM PC-AT. We added a uniform field to the screen using a pair of symmetrically placed slide projectors to increase the contrast resolution of the signal. We adjusted neutral density filters placed in the slide projectors' light path to keep their intensity level constant as the bulbs aged. The profiles of our spectral power distribution measurements for bulbs from any single manufacturer were the same throughout the experiment. The subject viewed stimuli through a restricting tube with a 10 deg square aperture that eliminated scattered light from the projectors and insured the 75 cm viewing distance.

The constant size condition. We presented stimuli on an Hitachi color monitor (model 4319) running at 60 Hz noninterlaced and controlled by a TrueVision video board (model ATVista) in an IBM PC-AT. To produce finer control of the video signals we passed the video board voltage output through special electronic circuitry (Poirson, 1991). Subjects viewed the screen from 1.82 m. The background subtended 7 deg.

2.3. Calibration

We measured the relative spectral power distributions of each of the three phosphors and also characterized the non-linear relationship between video board input and monitor output at regular bi-weekly intervals (Brainard, 1989). We also measured the monitors' modulation contrast function through the entire spatial frequency range of our experiments using a fast spatial scanner (Photo Research, model PR-719).

2.4. Psychometric function estimation

The psychometric function is the relationship between stimulus strength, $\|\mathbf{s}\|$, and the probability of correct detection. We approximate the psychometric function using the Weibull,

$$p = 1 - 0.5\exp[-(\|\mathbf{s}\|/\alpha)^\beta]. \qquad (5)$$

We estimate the psychometric function offset parameter, α, and slope parameter, β, in all the models we describe later by maximizing the likelihood function (Watson, 1979) using an iterative search procedure STEPIT (Chandler, 1965). We repeated all iterative searches several times, using different starting positions, to insure we obtained a global minimum.

2.5. Task overview

Two female subjects collected sensitivity measurements to vertically oriented, single frequency Gabor patches using a two-interval forced-choice (TIFC) procedure. An experimental session consisted of 128 or 144 trials in which the observer viewed two randomly interleaved staircases. The stimulus color direction and spatial pattern remained unchanged in a session. The data presented here represent more than 70,000 forced-choice decisions.

3. RESULTS

3.1. Overview of the three nested models

We evaluate how well our sensitivity measurements can be explained by fitting the data with three related models. The three models form a nested sequence in that each model in the sequence makes stronger assertions about the structure in the data and has correspondingly fewer free parameters than the preceding model. We describe the models qualitatively in the text, and we develop their mathematical formulations in the Appendix.

The *psychometric model* serves as a baseline measure of our ability to predict performance. In this model we fit separately a Weibull psychometric function to sensitivity data in each color direction and test pattern condition. Deviations from this model are due only to failures of the psychometric function shape and variability in the measurements. The psychometric model makes no assumptions about the relationship between data from different color directions or test pattern conditions.

The *pattern-dependent ellipsoid model* adds the assumption that for each test pattern, sensitivity to test lights in the different color directions are related. Specifically, the model is based on the idea that color coordinates of equally detectable stimuli fall on an ellipsoid in color space. There is a simple intuitive geometric interpretation of the pattern-dependent ellipsoid model. If the model holds, then it is possible to apply a linear transformation to the color coordinates such that equally detectable stimuli fall on a sphere. In this coordinate frame, the probability of detection is predicted by the vector-length of the stimulus representation (see

e.g. MacAdam, 1942; Wyszecki & Stiles, 1982, pp. 654–689; Wandell, 1982, 1985; Poirson et al., 1990). The pattern-dependent ellipsoid model posits a relationship between the sensitivity to stimuli of different colors and of a single test-pattern, but the model makes no assumptions relating the spatiochromatic sensitivity to different test patterns.

The *pattern–color separable model* adds the assumption that the three visual mechanisms mediating sensitivity are pattern–color separable. This is the strongest model, and it serves to test our main hypothesis. As we show in the Appendix this model predicts that there is a color coordinate frame in which the ellipsoidal detection contours share the same principal axes. In this coordinate frame, the directions of these principal axes are equal to the color sensitivity of the three visual mechanisms; the lengths of the axes are inversely related to the pattern sensitivity of the mechanism. Hence, by finding a color coordinate frame in which the principal axes of the ellipsoids align, we can estimate the unique pattern and color functions of the putative pattern–color separable visual mechanisms. The pattern–color separable model is the strongest of the models because it specifies the relationship between data with different test patterns and colors.

3.2. Evaluating the models

Figure 1 shows results from one test pattern condition and three different color directions. The symbols and smooth curves represent percent correct responses and fitted Weibull psychometric functions respectively. The vertical bars represent ±1 standard deviation away from the predicted probability correct. As we explain later, we use these standard deviations to equate errors between data having a different number of observations. In the psychometric model, the two psychometric function parameters are free to vary separately for each test-pattern and color direction. The psychometric functions fitted to these three data sets are typical of all of the psychometric functions we have observed. When represented in cone coordinates, sensitivity to different color directions varies by as much as an order of magnitude. The slopes of the psychometric functions for these colored, long-duration and medium spatial frequency patterns, as measured by the parameter β, are generally near 2.0. Later when reasoning with our data, we sometimes use the test vector that yields 82% correct detection on the psychometric function and call this threshold detection sensitivity.

We measure how well each model fits the detection data using a *normalized error* measure, which we compute as follows. For each test stimulus and model, we have an observed probability of correct detection, a predicted probability correct from the psychometric curve, and the number of observations at each test stimulus strength. Assuming that the responses are statistically independent, we can calculate the standard deviation of the binomial distribution at each stimulus strength given the number of observations and the
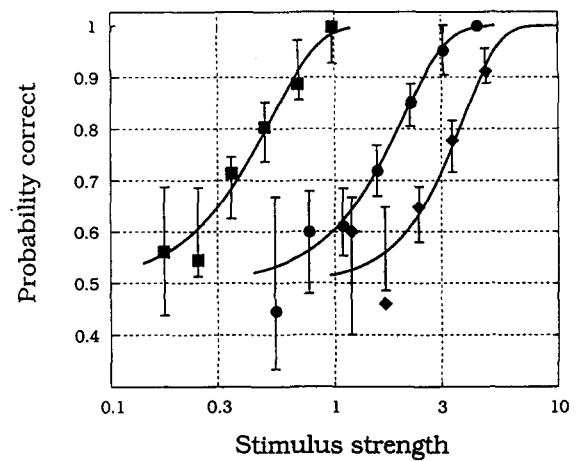

FIGURE 1. The probability of correct detection as a function of stimulus strength for stimuli in three color directions is shown. The smooth curves through the data show the best-fitting Weibull psychometric functions. The vertical bars plot ± 1.0 standard deviation of the probability correct predicted from the function. The stimulus spatial frequency was 4 c/deg (obs. HT, constant cycle condition). The three different curves and associated symbols show sensitivity to stimuli in the LMS color directions: (0,1,0), squares; (0.4, 0.4, 0.8), circles; (0,0,1), diamonds.

predicted probability of a correct response. We express the deviation of the observation from the prediction as the difference between the observed and predicted probabilities of correct detection, divided by the standard deviation. This we call the normalized error.

We evaluate the quality of the model fits by examining the normalized error from all of the sensitivity measurements. Figure 2(A) shows the distribution of normalized errors of the psychometric model for the two subjects in the constant size condition, and Fig. 2(D) shows the distribution of normalized errors for the one subject in the constant cycle condition. The horizontal axis represents normalized error and the vertical axis represents the number of conditions within each histogram bin. If the error can be explained by independent, binomial variability alone, and to the extent the normal approximation to the binomial is valid for our sample sizes, the histogram should follow the normal curve superimposed on the graph. In both conditions, and for all three subjects separately, the observed normalized error is better than the predicted unit normal curve. Presumably, this represents over-fitting of the data and a failure of the normal approximation for some small sample sizes. We believe, that there are too many free parameters in this model and that the psychometric model fits aspects of the data that arise merely because of chance fluctuations.

3.3. Evaluating the pattern-dependent ellipsoid model

The pattern-dependent ellipsoid model reduces the number of free parameters in two ways. First, the model assumes that there is an ellipsoidal relationship among the sensitivity parameters, α, for different color stimuli of the same pattern. Moreover, the slope parameter β is assumed to be the same for all colors with a common test pattern.
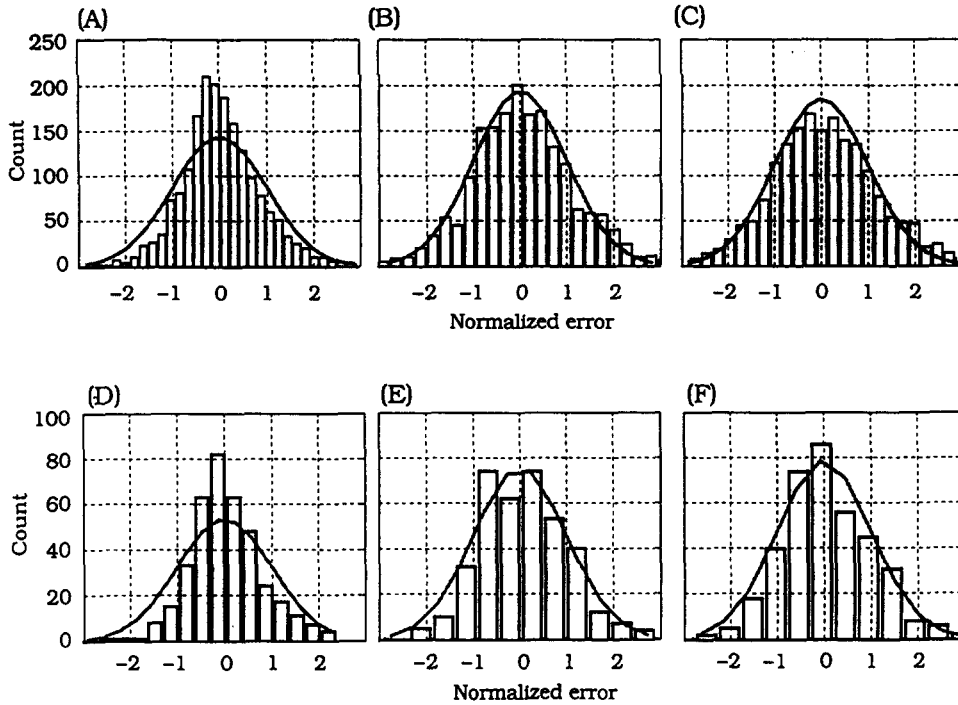
Figure 2(B) shows the normalized error histograms

FIGURE 2. Normalized errors of the different model fits are shown. Errors in the constant size condition are shown in the upper panels (A,B,C; obs. HT and LW) and errors in the constant cycle condition are shown in the lower three panels (D,E,F; obs. HT). (A,D) Histograms of the normalized errors of the psychometric model follow a normal curve that is narrower than the unit normal (shaded curve). (B,E) The normalized error histograms for the pattern-dependent ellipsoid model follow the unit normal curve closely. (C,F) The normalized error histograms of the pattern–color separable model are slightly wider than the unit normal, but not very different from it. See the text for details.

from fitting the pattern-dependent ellipsoid model for the constant size condition and 2(D) shows the distribution for the constant cycle condition. The normalized error frequency distributions have a slightly larger spread than the corresponding plot in the psychometric model, but in both cases, and for all three subjects when analyzed independently, the normalized error histograms of this model follow the standard normal distribution closely.

Because there is good agreement between the mea-

surements and the predictions of the pattern-dependent ellipsoid model, the shapes of the detection contours must fall close to ellipsoids when plotted in cone coordinates. We plot an example of such a detection contour in Fig. 3. We represent the three-dimensional data set in terms of three cross-sections in cone coordinates. The data points in this figure are taken from the constant cycle condition, using a 2 c/deg pattern. The data points represent threshold performance determined from psy-
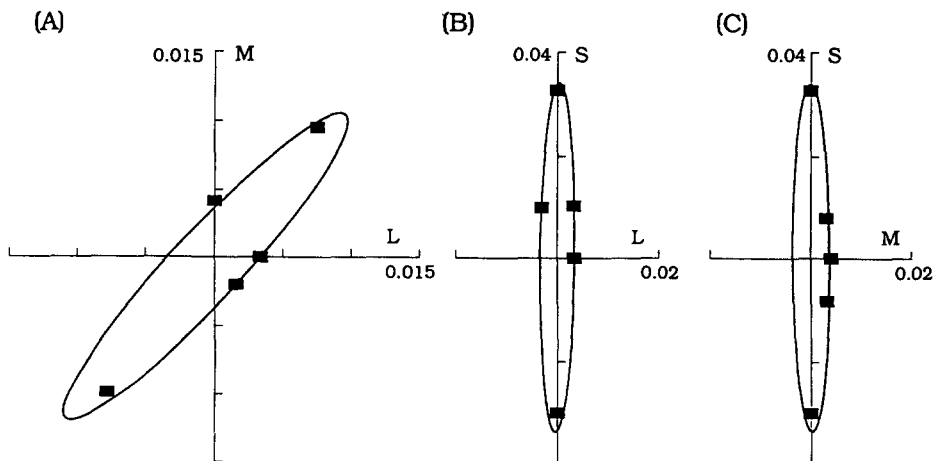

FIGURE 3. Threshold detection contours and observed threshold detection sensitivities are plotted in three cross-sections of cone coordinates. The solid curve in each panel shows a planar cross-section through the origin of the best-fitting ellipsoidal detection surface. The ellipsoid was estimated using the pattern-dependent ellipsoid model fit to all 20 data points measured using 2.0 c/deg patterns in the constant cycle condition (obs. HT). The data points show threshold detection estimated by fitting psychometric functions individually to data in eleven of the different color directions that happen to fall within one of cross-sections. (A) A cross-section in the (L, M) plane, (B) is a cross-section in the (L, S) plane, and (C) is in the (M, S) plane. The units are cone contrast.
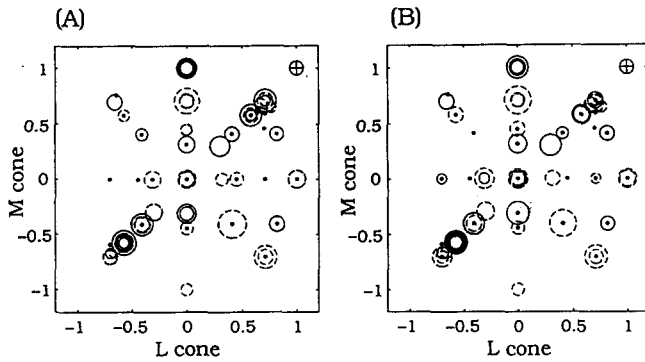
(A)   (B)

FIGURE 4. Difference between threshold detection sensitivity determined by the psychometric model and predictions from the pattern-dependent ellipsoid model (A) and the pattern–color separable model (B) at various cone coordinates. We indicate the test color direction by plotting the L-cone and M-cone values of the unit-length color–direction vector, s̄. [The color direction that stimulates only the S-cone plots at (0, 0).] The size of the error is shown by the circle diameter; solid and dashed circles denote predictions that are greater or less than the observation, respectively. Dots represent predictions that differ from the observation by less than 5%. The cross-hair circle in the upper right corner of each panel represents a 10% error. The pattern of errors are distributed similarly for the two models. Data are from subject HT in the constant cycle condition. See text for details.

chometric functions fit individually to data in eleven different color directions that lie in one of these planes. The smooth curves in each panel show the ellipse predicted by the best fitting pattern-dependent ellipsoid model. The ellipsoid is fit to measurements in all color directions, not just those measurements within the planes. Were the pattern-dependent ellipsoid model perfect, data points would fall precisely upon the ellipses. Visually, in this example and many others we have inspected, the data points fall close to the predicted ellipsoid. Hence, for each test pattern equally detectable stimuli fall upon an ellipsoid in color space.

3.4. Evaluating the pattern–color separable model

Next, we test the pattern–color separable model. Figure 2(C, F) show the normalized error distribution in the constant size and constant cycle condition respectively. In both conditions the distribution is slightly broader than the plotted standard normal curve and is quite similar to the distribution from the pattern-dependent ellipsoid model, which uses many more free parameters.

The pattern–color separable model's quality-of-fit is impressive considering how strongly it is constrained compared to the other two previous nested models. The pattern-dependent ellipsoid model uses seven parameters to fit the data for each test pattern, thus using 35 parameters to fit the constant size data. The pattern–color separable model relates all the ellipsoids, even those measured using different test patterns. The pattern–color separable model uses six parameters to determine the color space that applies to all patterns, three additional parameters for every test pattern, plus one slope parameter, β, for all the data. Hence, this model uses only 22 parameters to fit the entire data set. By comparing the normalized error histograms in Fig. 2, we find that the

quality-of-fit is only slightly worse for the separable model compared to the pattern-dependent model.

3.5. Comparing pattern dependent and pattern–color separable models

The normalized error histograms include data from all color and pattern conditions. Hence, these histograms provide an overview of how well the models describe performance. On the other hand, such an overview measure may mask systematic failures of the models in fitting certain test patterns or colors. A second way to examine how well the models fit is to study the pattern of the residual errors.

The two panels in Fig. 4 show the difference between threshold detection sensitivity determined by the psychometric model, and predictions from the best-fitting pattern-dependent ellipsoid model [Fig. 4(A)] and pattern–color separable model [Fig. 4(B)] for all the data collected in the constant cycle condition. In order to plot the three-dimensional measurements in a two dimensional graph, we use only the L-cone (x-axis) and M-cone (y-axis) values of the unit-length color–direction vector, s̄. In this representation, the color direction that stimulates only the S-cone plots at (0,0).

At each location we indicate larger errors in predicted threshold performance by larger circle diameters. We indicate the direction of the error by the circle linetype where solid and dashed circles denote predictions greater than and less than expected respectively. To simplify the figure, dots represent threshold performance data that fall within 5% of the prediction. Were all of the threshold measures to fall precisely upon the ellipsoids described by a model, all the errors would be represented by dots. The circle with a cross-hair in the upper right corner of each panel represents a 10% error.

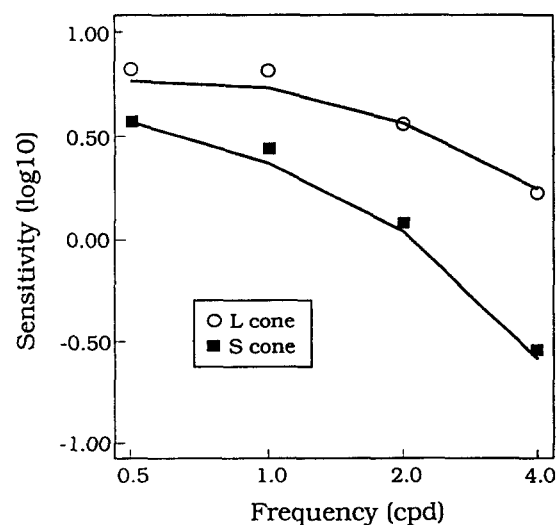We see no systematic difference between the two

FIGURE 5. Predicted and observed sensitivity measurements. The open circles and filled squares show threshold detection sensitivity to different spatial frequency stimuli in the L-cone and S-cone color directions, respectively. Solid lines represent the predicted threshold detection sensitivity based on the pattern–color separable model. The average difference between the model predictions and the measurements is 0.035 log units.

TABLE 1. Values of the color transformation matrix, T, for the best fitting pattern–color separable model

Subject	Function	L	M	S	Graph line type
HT, cc	W–B	0.759	0.649	0.058	Solid
	R–G	−0.653	0.756	0.033	Dashed
	B–Y	−0.159	−0.414	0.896	Dotted
HT, cs	W–B	−0.246	0.967	−0.072	Solid
	R–G	−0.698	0.716	−0.005	Dashed
	B–Y	0.165	−0.599	0.784	Dotted
LW, cs	W–B	0.717	0.677	−0.164	Solid
	R–G	−0.670	0.742	−0.029	Dashed
	B–Y	0.199	−0.682	0.703	Dotted

panels. Circle sizes and linetypes look similar in corresponding regions of the panels. This means that when one model misses the other model misses in the same direction and by the same amount. Furthermore, circle sizes are evenly distributed throughout both panels. This means that there are no color directions or color planes in which one model predicts the threshold performance data better overall. These results are similar for our two subjects in both conditions and hold when we compare plots from single test patterns as well. We conclude that the increase in error due to the stronger assertions we impose are distributed evenly throughout the data and does not provide just cause for rejecting the pattern–color separable model.

3.6. Predicted pattern sensitivity functions

As a third test of the pattern–color separable model, we used the estimated model parameters to predict subject HT's performance in the constant cycle condition to a new set of data. Specifically, we measured subject HT's pattern sensitivity functions to new test stimuli at several spatial frequencies in the L-cone (circles) and S-cone color directions (boxes). The threshold measurements are shown in Fig. 5 along with sensitivities predicted by the pattern–color separable model. The average difference between the model predictions and the measurements is 0.035 log units, which is about the size of the measurement error. The fitted model successfully predicts the new measurements.

3.7. Estimated separable color and pattern functions

The pattern–color separable model provides a reasonable description of the sensitivity data, with typical deviation in predicting the psychometric function data of only slightly more than one normalized error unit. The fit of the separable model is only slightly worse than the pattern-dependent model. The quality-of-fit, predictive ability and lack of patterned residuals of the pattern–color separable model all warrant exposition of the color and pattern functions that can be derived from the separable model.

---

* We represent the average results because the curves from the two subjects are quite similar. Fits to the data from the individual subjects can be obtained from the values in Table 1.

TABLE 2. Values of the spatial sensitivity matrices, D_f, for the best fitting pattern–color separable model

Subject	Frequency (c/deg)	W–B (solid)	R–G (dashed)	B–Y (dotted)
HT, cc	0.5	0.753	8.732	4.075
	1	1.226	8.044	2.567
	2	0.864	5.435	1.187
	4	0.683	2.536	0.266
HT, cs	0.5	11.864	63.945	8.080
	1	18.037	74.214	7.212
	2	23.739	60.598	3.235
	4	28.354	31.746	3.379
	8	26.959	12.302	2.622
LW, cs	0.5	4.981	60.556	6.575
	1	6.406	53.460	5.390
	2	11.081	36.944	3.785
	4	12.354	24.390	2.747
	8	9.550	19.513	3.706

As we described earlier in the text, and we show quantitatively in the Appendix, the visual mechanisms estimated by the fit of the pattern–color separable are summarized in two linear transformations and the slope of the psychometric functions, β. The color sensitivity is described by a linear transformation that converts the stimulus cone absorptions into a new color coordinate frame. The pattern sensitivities associated with each of the visual mechanisms is described by a diagonal linear transformation whose entries are pattern-dependent functions and serve to scale the axes of the new color representation. We have tabulated the entries of the color transformation (Table 1), pattern-dependent functions (Table 2), and the psychometric function slopes (Table 3) for each subject separately.

To provide an intuitive graphical representation of the color functions, we can plot the relative wavelength sensitivity of the axes in the estimated color coordinate frame. Figure 6(A) shows the average of the wavelength sensitivity functions from the two subjects in the constant size condition.* It is of interest to note that although we made no a priori assumptions about the form of these mechanisms, still they can be classified into one broadband mechanism and two spectrally opponent mechanisms. These functions are quite similar to classically defined opponent mechanisms measured using procedures such as hue cancellation (e.g. Hurvich & Jameson, 1957). Without implying that these functions are precisely the same as the ones obtained in those experiments, we will refer to these functions as white–

TABLE 3. Slope parameters, β, for the best fitting pattern-dependent ellipsoid and pattern–color separable models

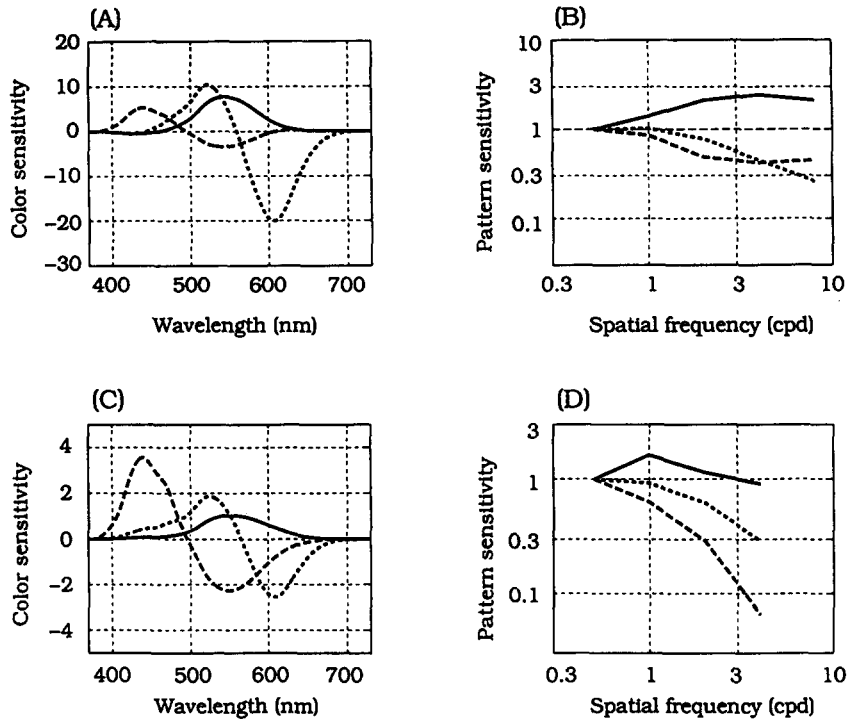| Model	Frequency (c/deg)	HT,cc	HT,cs	LW,cs
PDE	0.5	1.86	1.70	1.55
PDE	1	1.84	1.70	1.85
PDE	2	1.97	2.26	2.42
PDE	4	2.18	2.42	2.42
PDE	8	—	2.52	2.01
PCS	all	1.95	1.82	1.94

FIGURE 6. Color and pattern sensitivity functions derived from the data in the constant size (upper panels) and constant cycle (lower panels) conditions. (A) The average wavelength sensitivity functions of three mechanisms estimated from the data of HT and LW in the constant size condition are shown. The solid curve shows the sensitivity of the white–black mechanism, the dotted curve shows the red–green mechanism, and the dashed curve shows the blue–yellow. (B) The pattern sensitivity functions of the same three mechanisms, estimated in the constant size condition. (C) The color sensitivity functions and the (D) pattern sensitivity functions for the mechanisms estimated from observer HT's data in the constant cycle condition are shown. In all panels, the color and pattern functions of a single mechanism are drawn using the same linetype. The units are normalized so that each mechanism's sensitivity at 0.5 c/deg is 1.0. See the text for details.

black (solid line), red–green (dashed line) and blue–yellow (dotted line) color functions.

Figure 6(B) shows the pattern sensitivity functions estimated in the constant size condition using the separable model. Each pattern sensitivity function is associated with one of the three color mechanisms. The white–black function shows a bandpass characteristic peaking near 4 c/deg in the constant cycle condition. The red–green and blue–yellow pattern sensitivities are both lowpass.

Subject HT collected data in both the constant cycle and constant size conditions. Figure 6(C) shows the color functions derived from fitting the separable model to her constant cycle data. Qualitatively, the color functions derived in the two different conditions are quite similar. The zero-crossings of the functions fall at approximately the same wavelengths. The functions differ mainly by a scale factor, as might be expected given the very different spatial patterns and adapting conditions that were used in these experiments.

The pattern sensitivity functions estimated in the constant cycle condition [Fig. 6(D)] differ from those estimated in the constant size condition in two significant ways. First, subject HT was more sensitive in the constant size condition. Second, the pattern sensitivity functions fall off more rapidly with spatial frequency in the constant cycle condition. Qualitatively, these differences in the pattern function are expected based on the differences in the stimulus conditions, namely that the

background intensity in the constant cycle condition was ten times higher than in the constant size condition, and the area of the test stimuli differed between these two conditions. Increasing the background intensity decreases spatial pattern sensitivity, while increasing the number of spatial cycles in the stimulus increases pattern sensitivity (see Graham, 1989).

We make a somewhat sharper comparison based on the following arguments. We can adjust the pattern sensitivity for the change in background intensity by shifting the constant cycle functions (on a logarithmic axis) so that corresponding curves coincide at 2.0 c/deg, since at this frequency the stimulus had approximately the same spatial extent and number of cycles in both test conditions. The remaining sensitivity differences should be due to the area of test stimuli. At spatial frequencies greater than 2 c/deg, the constant cycle stimuli occupy a much smaller area of the visual field than the constant size stimuli, while at lower spatial frequencies the reverse is true. When we shift the curves in this way, it becomes clear that within a given color pathway the subject is more sensitive to the spatial stimulus that covers the larger area. Thus, most of the differences in the shapes of the pattern sensitivity functions are probably due to the differences in the stimulus area (Howell & Hess, 1978; Noorlander, Heuts & Koenderink, 1980).

Finally, we note that our derived pattern and color functions serve to describe our subjects' sensitivity starting with a description of the stimulus on the display

device. Chromatic aberration within the eye will produce large changes in the retinal image, especially for the S-cones (see e.g. Marimont & Wandell, 1993). Can we factor out the influence of purely optical components, the cornea and lens, on these functions? To do this we need to estimate the retinal signal of our stimuli and use these values in our pattern–color separable analyses. In our earlier study (Poirson & Wandell, 1993) we found that axial chromatic aberration was the primary cause for the loss of spatial resolution. Unfortunately in this study, after estimating the retinal signal, we find that the data no longer serve to constrain the parameters of our model adequately and yield unstable parameter estimates. Anticipating the impact of chromatic aberration while collecting data is important in order to adequately sample retinal color space and constrain our model.
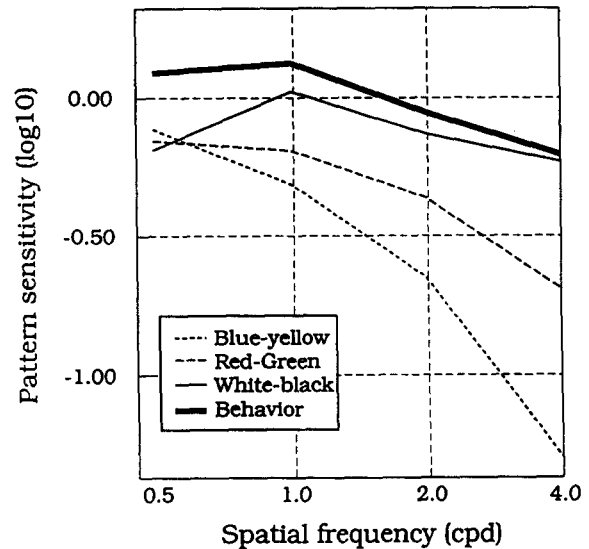

FIGURE 7. The predicted behavioral pattern sensitivity (thick solid curve) and the relative contributions to pattern sensitivity by three estimated mechanisms are shown. The behavioral prediction and the individual mechanism sensitivities are based on the best-fitting pattern–color separable model in the constant cycle condition (HT,cc). The estimates are based on a test color direction (ŝ = 1/√3, 1/√3, 1/√3). The solid, dashed and dotted lines show the contribution to the overall pattern sensitivity by the white–black, red–green and blue–yellow mechanisms respectively.

4. DISCUSSION

The pattern–color separable model provides a framework for thinking about how different visual pathways might contribute to visual sensitivity. Specifically, we can calculate how the mechanisms estimated by the model each contribute in predicting the subject's sensitivity to different spatiochromatic stimuli. In this section, we analyze the contribution of the different estimated mechanisms in two types of experiments. First, we estimate how the separate visual mechanisms contribute to the subject's pattern sensitivity curve for patterns that all share a common color direction. Second, we estimate how the separate visual mechanisms contribute to color sensitivity measured using a single test pattern. We use the pattern–color separable model fitted to subject HT's data in the constant cycle condition in our analysis.

4.1. Mechanism contributions to pattern sensitivity

Using the pattern–color separable model, it is possible to estimate how each of the individual visual mechanism contributes to pattern sensitivity. Figure 7 shows the relative contributions of the different mechanisms for various test patterns in the color direction, (ŝ = 1/√3, 1/√3, 1/√3). The thick solid line shows the predicted behavioral pattern sensitivity function. The thin solid, dashed and dotted curves falling below the performance prediction represent the contribution of the three pattern–color separable mechanisms.

It is possible to make a comparable figure for any color direction. As the color direction varies, the shape of the predicted pattern sensitivity function varies. Since the mechanisms are pattern–color separable, the shapes of the underlying pattern sensitivity functions remain the same; only their relative vertical position change to yield a different overall performance curve.

As we see from Fig. 7, all color pathways can contribute to pattern sensitivity measurements made using conventional methods, particularly in the low spatial frequency regime. To measure the pattern sensitivity of one mechanism alone, we would need to use lights in color directions that do not stimulate the two

unwanted mechanisms. In our conditions, we can estimate these color directions from the color transformation matrix in Table 1. For example, to isolate a response from the white–black pathway, one should choose a stimulus with color direction close to (0.70, 0.59, 0.40) because this is the only color direction that simultaneously silences the red–green and blue–yellow mechanisms.

In our conditions, the stimulus that isolates the white–black pathway is not equal to a modulation of the background light intensity. This is a disturbing observation because modulation of the background light intensity is the conventional stimulus used to measure pattern sensitivity. In our experiments, the color direction of the background light is (0.76, 0.60, 0.24), and this stimulus evokes a response in all three mechanisms. Using a 0.5 c/deg test pattern, the relative excitation of the white–black, red–green and blue–yellow mechanisms of an intensity modulation of the background is (0.72, −0.30, −0.63).

By examining the contributions of the different color mechanisms to pattern sensitivity in Fig. 7, we can see that the pattern–color separable model is a multiple spatial frequency channels model: three separate pathways coexist within a single region of the visual field, and each pathway has a different pattern sensitivity. This is not the same, however, as conventional multiresolution models (e.g. Campbell & Robson, 1968; Graham & Nachmias, 1971) in which the pattern sensitivity in one color direction requires a multiresolution representation. In our modeling the different spatial resolutions covary with the mechanism color sensitivities. We have not
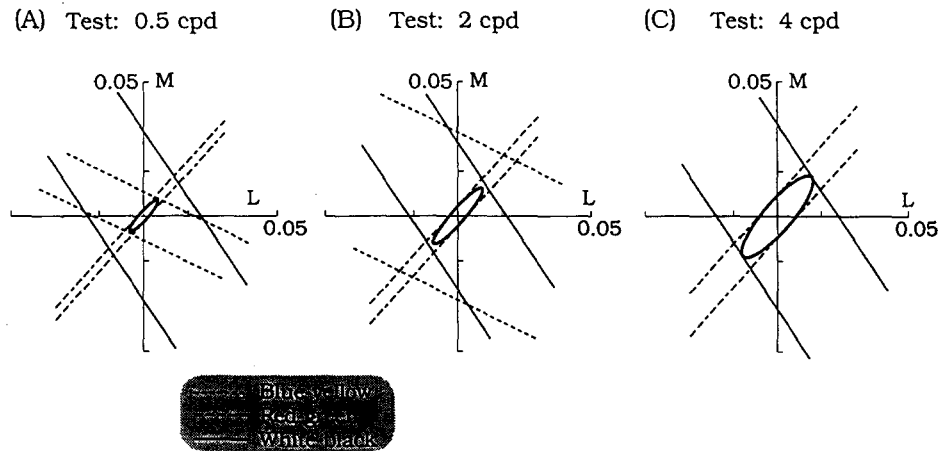
(A) Test: 0.5 cpd   (B) Test: 2 cpd   (C) Test: 4 cpd

FIGURE 8. The predicted behavioral color sensitivity (solid ellipses) and the relative contributions to sensitivity by three estimated pattern–color separable mechanisms are shown. The predicted behavioral sensitivity and the mechanism sensitivities are plotted in the (L, M) plane, representing a cross-section of the full three-dimensional predictions. Each mechanism's contribution to visual sensitivity can be estimated by how closely the lines bound the elliptical detection contour. The different visual mechanisms are shown using the solid, dotted and dashed line types as in previous figures. (A,B,C) Predictions for test patterns at 0.5, 2.0 and 4.0 c/deg respectively. Because mechanisms are pattern–color separable, the mechanism threshold contours always plot at the same orientation, changing only their distance from the origin with the test pattern. The units are cone contrast. See the text for details.

included such within pathway channels in our analyses because the fit to our data set without postulating these additional channels seems adequate (cf. Fig. 2), and we do not have the additional data that might allow us to test this idea within a pattern-color separable framework.

4.2. Mechanism contributions to color sensitivity

Just as it is possible to explain channel contributions to sensitivity measured at various spatial frequencies for a fixed color direction, so too we can separate out channel contributions to sensitivity measured in different color directions for a fixed spatial pattern. For this exposition we must visualize the sensitivity of the underlying visual mechanisms in three dimensional color space.

Suppose we have a visual system composed of one pattern–color separable mechanism that responds only to L-cone stimulation. Detection occurs when the stimulus increases or decreases the L-cone response by a criterion amount, Δ. The set of stimuli at detection threshold fall upon a pair of planes perpendicular to the L-cone axis. One plane represents mechanism threshold for stimulus increments (L = +Δ) and the second plane represents threshold for decrements (L = −Δ). If the mechanism spectral sensitivity depends on a weighted sum of signals from the three cone types, the orientation of the planes will change. Hence, the separation between the planes is the geometric counterpart of the mechanism's pattern sensitivity, and the orientation of the planes is the geometric counterpart of the mechanism's color sensitivity.

The pattern–color separable model has three visual mechanisms and therefore three pairs of parallel mechanism planes. Because signals from the mechanisms are combined using a vector-length rule, equally detectable test vectors are predicted to fall upon an ellipsoidal surface bounded by the mechanism planes.

It is difficult to visualize the six planes and the ellipsoid in a two-dimensional drawing, but it is possible to get a sense of the geometric relationship between these entities by examining planar cross-sections. For example, Fig. 8 shows the cross-section of this three-dimensional picture in the (L-cone, M-cone) color plane. In cross-section the ellipsoids become ellipses and the parallel planes become parallel lines.

Figure 8(A) shows that for the 0.5 c/deg pattern, thresholds in the (L, M) color plane are determined mainly by signals from the blue–yellow and red–green mechanisms. The parallel lines representing the sensitivity of the white–black mechanism are fairly far from the ellipse indicating that this mechanism contributes very little to the observer's sensitivity for most of the plotted color directions. Figure 8(B) shows that for the 2.0 c/deg pattern the ellipse is now bounded by the parallel planes corresponding to the red–green and white–black mechanisms; the blue–yellow mechanism is quite distant. This trend continues so that when the test is 4.0 c/deg [Fig. 8(C)] the blue–yellow mechanism does not even appear within the graph.

These plots show how the three mechanisms contribute to the visibility of the different frequency test patterns. For all three patterns, the red–green mechanism determines sensitivity for color directions perpendicular to the major axis of the ellipse. For the 0.5 c/deg target, the blue–yellow mechanism determines sensitivity in the direction perpendicular to the minor axis, while for the higher frequency targets the white–black mechanism determines sensitivity in these color directions. Notice that across the different panels in Fig. 8 the orientation of the lines representing the different mechanisms remains constant. The unchanging orientation of these lines is the geometric counterpart of pattern–color separability. Changing the test pattern alters the separation between

the lines corresponding to the mechanism's pattern sensitivity. But each mechanism's color sensitivity, indicated by the orientation of the lines, remains invariant as the pattern changes.

The graphs in Fig. 8 show that across these measurement conditions, we expect that the basic orientation of the elliptical detection contour will remain the same; the contour only changes in size. However, the visual mechanisms determining sensitivity do change significantly. This graph makes plain one of the logical difficulties in trying to infer visual mechanisms from the shape of one ellipsoid alone (e.g. Chaparro, Stromeyer, Huang, Kronauer & Eskew, 1993).

5. CONCLUSION

We began this paper by asking how pattern and color information are organized jointly within the visual system. Our measurements of pattern–color sensation are explained by the responses of three pattern–color separable mechanisms combined using a vector-length decision rule. Separability implies that pattern and color information are represented simultaneously in the separate pathway responses, without confound. To estimate color responsivity, then, one need not be concerned about the stimulus pattern. To estimate pattern responsivity, one need not be concerned about the stimulus wavelength. This is a sensible and efficient organization.

We have derived the spectral and spatial tuning functions of the pattern–color separable visual mechanisms using all of our sensitivity measurements. Neither our experimental methods nor our data analyses presupposes a second site opponent-colors representation of wavelength, yet our derived spectral functions are characteristic of white–black, red–green and blue–yellow responsivity. We use the model to estimate the contribution of each component mechanism to overall performance in one color direction and different test patterns (Fig. 7) and also for fixed test patterns and different color directions (Fig. 8).

Obtaining pattern–color separability from the responses of peripheral neurons is no easy computational task. Axial chromatic aberration and the spatial receptive fields of retinal ganglion cells serve to confound color and pattern information. Yet, the performance of our observers is consistent with a representation in which the pattern and color information is separable once again. Our results suggest that identifying the neuronal substrates of pattern–color separable responses will bring us closer to the neuronal representation of visual appearance.

REFERENCES

Boynton, R. M. (1979). *Human color vision*. New York: Holt, Rinehart and Winston.

Brainard, D. H. (1989). Calibration of a computer controlled color monitor. *Color Research and Application, 14*, 23–34.

Campbell, F. W. & Robson, J. G. (1968). Application of Fourier analysis to the visibility of gratings. *Journal of Physiology, 197*, 551–566.

Chandler, J. P. (1965). *STEPIT*. Indiana University, Bloomington, Indiana, U.S.A.: Quantum Chemistry Program Exchange, Department of Chemistry.

Chaparro, A., Stromeyer III, C. F., Huang, E. P., Kronauer, R. E. & Eskew, Jr, R. T. (1993). Colour is what the eye sees best. *Nature, 361*, 348–350.

Derrington, A. M., Krauskopf, J. & Lennie, P. (1984). Chromatic mechanisms in lateral geniculate nucleus of macaque. *Journal of Physiology, 357*, 241–265.

Finkelstein, M. A. & Hood, D. C. (1984). Detection and discrimination of small, brief lights: Variable tuning of opponent channels. *Vision Research, 24*, 175–182.

Gouras, P. (1968). Identification of cone mechanisms in monkey ganglion cells. *Journal of Physiology, 199*, 533–547.

Graham, N. (1989). *Visual pattern analyzers*. New York: Oxford University Press.

Graham, N. & Nachmias, J. (1971). Detection of grating patterns containing two spatial frequencies: A comparison of single-channel and multiple-channel models. *Vision Research, 11*, 251–259.

Granger, E. M. & Heurtley, J. C. (1973). Visual chromatic modulation transfer function. *Journal of the Optical Society of America, 63*, 73–74.

Hood, D. C. & Finkelstein, M. A. (1983). A case for the revision of textbook models of color vision: The detection and appearance of small brief lights. In J. D. Mollon & L. T. Sharpe (Eds), *Color vision* (pp. 385–398). London: Academic Press.

van der Horst, G. J. C. & Bouman, M. A. (1969). Spatio-temporal chromaticity discrimination. *Journal of the Optical Society of America, 59*, 1482–1488.

Howell, E. R. & Hess, R. F. (1978). The functional area for summation to threshold for sinusoidal gratings. *Vision Research, 18*, 369–374.

Hurvich, L. M. & Jameson, D. (1957). An opponent-process theory of color vision. *Psychological Review, 64*, 384–404.

Ingling Jr, C. R. & Martinez-Uriegas, E. (1985). The spatiotemporal properties of the r–g x-cell channel. *Vision Research, 25*, 33–38.

Knoblauch, K. & Maloney, L. T. (1996). Testing the indeterminacy of linear color mechanisms from color discrimination data. *Vision Research, 36*, 295–306.

MacAdam, D. L. (1942). Visual sensitivities to color differences in daylight. *Journal of the Optical Society of America, 32*, 247–274.

Marimont, D. & Wandell, B. (1993). Matching color images: The effects of axial chromatic aberration. *Journal of the Optical Society of America A, 12*, 3113–3122.

Marr, D. (1982). *Vision*. San Francisco: W. H. Freeman.

Mullen, K. (1985). The contrast sensitivity of human colour vision to red–green and blue–yellow chromatic gratings. *Journal of Physiology, 359*, 381–400.

Noorlander, C. & Koenderink, J. J. (1983). Spatial and temporal discrimination ellipsoids in color space. *Journal of the Optical Society of America, 73*, 1533–1543.

Noorlander, C., Heuts, M. J. G. & Koenderink, J. J. (1980). Influence of the target size on the detection threshold for luminance and chromaticity contrast. *Journal of the Optical Society of America, 70*, 1116–1121.

Poirson, A. B. (1991). Appearance and detection of colored patterns. Unpublished doctoral dissertation, Stanford University, Psychology Department.

Poirson, A. & Wandell, B. (1993). Appearance of colored patterns: Pattern–color separability. *Journal of the Optical Society of America, 10*, 2458–2470.

Poirson, A. B., Wandell, B. A., Varner, D. & Brainard, D. H. (1990). Surface characterizations of color thresholds. *Journal of the Optical Society of America, 7*, 783–789.

Smith, V. & Pokorny, J. (1975). Spectral sensitivity of the foveal cone photopigments between 400 and 500 nm. *Vision Research, 15*, 161–171.

Wandell, B. (1995). *Foundations of vision*. Sunderland, MA: Sinauer Associates.

Wandell, B. A. (1982). Measurements of small color differences. *Psychological Review, 89*, 281–302.

Wandell, B. A. (1985). Color measurement and discrimination. *Journal of the Optical Society of America A, 2*, 62–71.

Watson, A. B. (1979). Probability summation over time. *Vision Research, 19*, 515–522.

Wiesel, T. N. & Hubel, D. H. (1966). Spatial and chromatic interactions in the lateral geniculate body of the rhesus monkey. *Journal of Neurophysiology, 29*, 1115–1156.

Wyszecki, G. & Stiles, W. S. (1982). *Color science* (2nd edn). New York: John Wiley and Sons.

APPENDIX

Formal Description of the Models

Pattern-dependent ellipsoid model

The pattern-dependent ellipsoid model assumes that for each pattern there is a color coordinate frame in which the sensitivity to a color stimulus depends only on its vector-length. This model has been described and evaluated by Poirson *et al.* (1990), Knoblauch and Maloney (1996) and others cited therein.

Specifically, we apply a pattern-dependent linear transformation, A_f, to the test stimulus, $A_f s$, and compute the vector-length by,

$$\|A_f s\| = ([A_f s]^t [A_f s])^{\frac{1}{2}} = \|s\|(\bar{s}^t A_f^t A_f \bar{s} = \|\bar{s}\| s^t Q_f \bar{s})^{\frac{1}{2}} \quad (A1)$$

where $Q_f = A_f^t A_f$. The vector-length in the transformed coordinate frame is proportional to the vector-length in the initial coordinate frame. The constant of proportionality is $(\bar{s}^t Q_f \bar{s})^{-\frac{1}{2}}$.

To test the pattern-dependent ellipsoid model we substitute $\alpha = (\bar{s}^t Q_f \bar{s})^{-\frac{1}{2}}$ in equation (5) and estimate the six parameters of the quadratic, Q_f, and the one slope parameter, β. We analyze the data from each test pattern, f, separately. Notice that the quadratic form specifies the offset parameter, α, for each color direction. This allows us to fit one psychometric function to sensitivity data measured in more than one color direction. The pattern-dependent ellipsoid model is stronger than the psychometric model since β and the six parameters determining α are the same for every color direction; these parameters depend only on the spatial pattern of the test.

As we have explained elsewhere, when we fit a quadratic model to a collection of threshold data using a single pattern, we recover a unique estimate of the quadratic, Q_f. We cannot, however, recover a unique estimate of the linear transformation, A_f (Poirson *et al.*, 1990). Hence, the pattern-dependent ellipsoid model does not permit us to estimate uniquely a set of mechanisms determined by the transformation, A_f. We can estimate this transformation by fitting data from all test patterns simultaneously, as we do in the next model.

Pattern–color separable model

The pattern–color separable model extends the pattern-dependent ellipsoid model by assuming that the collection of linear transformations, A_f, are all related. Specifically, we assume that all of the linear transformations can be described as a single color transformation that is independent of the test pattern, followed by a scaling of the new color function responsivities by factors that depend only on the test pattern frequency.

The independence of the color and pattern transformations implies that the matrix A_f in equation (A1) can be factored into two terms,

$$A_f = D_f T. \quad (A2)$$

The color matrix T defines a transformation from the original receptor absorptions into new color function responses. This matrix is fixed and independent of the stimulus. The diagonal second matrix, D_f, scales each of the axes in the new color coordinate frame and depends on the test pattern, f. We can express the quadratic form of the pattern–color separable model in terms of the two matrices, D_f and T, such that

$$Q'_f = (D_f T)^t (D_f T). \quad (A3)$$

To test the pattern–color separable model we use the restricted pattern–color separable quadratic, Q'_f, instead of the general quadratic, Q_f, in equation (A1). Analogous to the pattern-dependent ellipsoid model, we substitute the psychometric function offset parameter, α, with $(\bar{s}^t Q'_f \bar{s})^{-\frac{1}{2}}$. We search for the six parameters of the color matrix T, the entries in the diagonal matrices D_f, and the one slope parameter, β, to fit this model to a subject's entire data set.

The pattern–color separable model is stronger than the pattern-dependent ellipsoid model for two reasons. First, all of the quadratics, Q'_f, must be decomposable into the form given in equation (A3) and share the same color transformation T. Second, we use the same slope parameter, β, for all different test pattern frequencies. The condition that the axes of the ellipsoidal iso-detection surfaces from different test patterns must align is equivalent to saying that all of the quadratics describing the surfaces must share the common color transformation T.

Estimating the color and pattern functions

The parameters in matrix T define the three mechanisms' color functions. We calculate a mechanism's spectral responsivity as follows. Suppose t_{ij} is the ijth entry of T. The ith mechanism's spectral responsivity is then $t_{i1}L(\lambda) + t_{i2}M(\lambda) + t_{i3}S(\lambda)$.

The mechanisms' pattern sensitivities are given by the diagonal matrices D_f. The (1, 1) entry in the D_f matrices define the pattern sensitivity for the color function defined by the first row of matrix T and pattern f. The second and third pathways' pattern sensitivities are defined by the (2, 2) and (3, 3) entries respectively.

The relative values of the color and pattern functions are unique. The absolute values of the color and pattern sensitivities are not unique. Any vertical shift in a given pattern sensitivity can be compensated by scaling the sensitivity of the corresponding color function. We have chosen to scale the pattern functions in Fig. 6 so that amplitude sensitivity at 0.5 c/deg equals 1.0.